Effects of the surface boundary on the magnetization process in type-II superconductors

Ryuzo Kato
Department of Applied Physics, Nagoya University, Nagoya 464-01, Japan

Yoshihisa Enomoto*
Department of Physics, Nagoya University, Nagoya 464-01, Japan

Sadamichi Maekawa
Department of Applied Physics, Nagoya University, Nagoya 464-01 Japan
(Received 27 July 1992; revised manuscript received 30 October 1992)

Computer simulations, based on the time-dependent Ginzburg-Landau equation of the magnetization process of type-II superconductors in a magnetic field are presented. It is shown how the magnetic flux penetrates into and goes out of the superconductor through the surface boundary, i.e., the superconductor-insulator interface. By examining the hysteresis curve of the magnetization, the surface pinning field is derived. The flux distribution and its time development in the superconductor are calculated when the magnetic field is increased or decreased. We also study the surface and edge states of the type-II superconductor above the upper critical field.

I. INTRODUCTION

A variety of the anomalous electromagnetic phenomena of type-II superconductors have received much attention, particularly since the discovery of high-temperature superconductors. Several phenomenological theories were applied to analyze the irreversible phenomena. The phenomena are related to the dynamical properties of magnetic vortices. Since the dynamics are sensitively dependent on the details of the superconducting materials such as sample surfaces and inhomogeneities, it is complicated and difficult to examine the phenomena based on the microscopic model.

Recently, three kinds of computer-simulation methods have been applied to the study of the vortex state based on the semimicroscopic models: (i) the Monte Carlo simulation based on the Ginzburg-Landau free-energy functional with a simulated annealing method,[1] (ii) the molecular-dynamics annealing simulation based on the Langevin equation for vortices,[2,3] and (iii) the difference method to solve the time-dependent Ginzburg-Landau (TDGL) equation.[4–6] In a previous paper,[4] we have proposed that the third method is particularly useful to investigate the dynamics of magnetic flux in type-II superconductors, since external conditions such as the time-dependent magnetic field and sample geometry can be introduced into the equation as parameters. We have presented the simulations of the nucleation process of the superconducting state with and without an external magnetic field starting with the normal state, the pair annihilation of a vortex and an antivortex, and the pinning process of a vortex by an impurity.

In this paper, we extend the method of Ref. 4 and study the magnetization process of type-II superconductors with the surface boundary, i.e., the superconductor-insulator interface, in the wide range of the external magnetic field. Bean and Livingston[7] have presented the phenomenological model for the surface pinning of vortices and proposed the characteristic magnetic field for the magnetic-flux penetration into type-II superconductors. This field is much higher than the lower critical field H_{c1}. We study the magnetization process and derive the field based on the TDGL equation. We also examine the surface superconducting states and find the edge states that exist even above the surface critical field[8] H_{c3}.

In Sec. II we briefly review the TDGL equation. A gauge transformation for eliminating the scalar potential and the link variable[5] for treating the vector potential are introduced. In Sec. III the simulation method to solve the TDGL equation is presented. In Sec. IV the method is applied to the magnetization process of type-II superconductors. Starting with the zero-field cooling (ZFC) state, we examine the time development of the magnetization and observe how the magnetic flux penetrates into and goes out of the superconductors through the surface boundary. In Sec. V the hysteresis curve of the magnetization and surface and edge states are derived. The results of the simulation are summarized in Sec. VI. In the text, normalized units introduced in Sec. II are used unless noted, whereas the figures are shown in physical units.

II. TIME-DEPENDENT GINZBURG-LANDAU EQUATION

In this section, we review briefly the TDGL equation and set up the formalism necessary for examining the magnetization process in type-II superconductors. The TDGL equation is a partial differential equation for the space and time dependence of the complex order parameter $\Delta(\mathbf{r})$ and the vector potential $\mathbf{A}(\mathbf{r})$. It is conveniently written in the normalized form as[9]

$$D^{-1}\left[\frac{\partial}{\partial t}+i\frac{2e\psi}{\hbar}\right]\Delta=-\left[\frac{\nabla}{i}-\frac{2e}{\hbar c}\mathbf{A}\right]^2\Delta-\xi(T)^{-2}(|\Delta|^2-1)\Delta+f(\mathbf{r},t)\ ,$$
$$\mathbf{j}=\sigma\left[-\nabla\psi-\frac{1}{c}\frac{\partial\mathbf{A}}{\partial t}\right]+\mathrm{Re}\left[\Delta^*\left[\frac{\nabla}{i}-\frac{2e}{\hbar c}\mathbf{A}\right]\Delta\right]\frac{\hbar c^2}{8\pi e\lambda(T)^2}\ , \tag{1}$$

where $\psi(\mathbf{r})$ is a scalar potential, $f(\mathbf{r},t)$ is the random force,[10] and $\mathbf{j}(\mathbf{r})$ is the total current density. Here, we have neglected the displacement current and the difference between the scalar potential and the electrochemical potential, assuming both are small.[11] The order parameter Δ is divided by its equilibrium value in the absence of the magnetic field, i.e., $\Delta_\infty=[mc^2/8\pi e^2\lambda(T)^2]^{1/2}$. Here, D and σ are the normal-state diffusion constant and conductivity, respectively, and are given in the microscopic theory by

$$\frac{4\pi\lambda(T)^2\sigma}{c^2}=\frac{\xi(T)^2}{12D}=\frac{\pi\hbar}{96k_BT_c}\left[1-\frac{T}{T_c}\right]^{-1}\equiv t_0\left[1-\frac{T}{T_c}\right]^{-1}\ , \tag{2}$$

where T_c is the critical temperature and t_0 is the characteristic time for the order parameter defined by $t_0\equiv\pi\hbar/96k_BT_c$. The coherence length $\xi(T)$ and the magnetic penetration depth $\lambda(T)$ are given by

$$\xi(T)=\xi(0)\left[1-\frac{T}{T_c}\right]^{-1/2}\ ,$$
$$\lambda(T)=\lambda(0)\left[1-\frac{T}{T_c}\right]^{-1/2}\ , \tag{3}$$

respectively. Thus, the Ginzburg-Landau parameter $\kappa\equiv\lambda(T)/\xi(T)$ is independent of temperature. In Eqs. (1)–(3), the other notations are the conventional ones. The random force is uncorrelated in space and time,

$$\langle f^*(\mathbf{r},t)f(\mathbf{r}',t')\rangle=12\xi(0)^{-4}t_0k_BT\left[\frac{H_c(0)^2}{8\pi}\right]^{-1}\times\delta(\mathbf{r}-\mathbf{r}')\delta(t-t')\ , \tag{4}$$

where $\langle\cdots\rangle$ denotes the ensemble average and $H_c(0)$ is the thermodynamic critical field at $T=0$.

Let us introduce a gauge transformation of the scalar and vector potentials,

$$\mathbf{A}\rightarrow\mathbf{A}-\nabla\chi,\quad\psi\rightarrow\psi+\frac{1}{c}\frac{\partial\chi}{\partial t}\ , \tag{5}$$

accompanied by a phase redefinition of the order parameter

$$\Delta\rightarrow\Delta\exp\left[-i\frac{2e}{\hbar c}\chi\right]\ . \tag{6}$$

Then, setting[4] $\partial\chi/\partial t=c\psi$, we eliminate the scalar potential in the TDGL and Maxwell equations. The equations can be rescaled as follows:

$$\begin{aligned}&\mathbf{r}\text{ in units of }\xi(0)\ ,\\ &t\text{ in units of }t_0\ ,\\ &\mathbf{A}\text{ in units of }H_{c2}(0)\xi(0)\ ,\end{aligned} \tag{7}$$

where the upper critical field is given by $H_{c2}(T)=H_{c2}(0)(1-T/T_c)$. In normalized units, the TDGL equation is rewritten as

$$\frac{\partial\Delta}{\partial t}=-\frac{1}{12}\left[\left[\frac{\nabla}{i}-\mathbf{A}\right]^2\Delta+(1-T)(|\Delta|^2-1)\Delta\right]+\tilde{f}(\mathbf{r},t)\ , \tag{8}$$

$$\frac{\partial\mathbf{A}}{\partial t}=(1-T)\mathrm{Re}\left[\Delta^*\left[\frac{\nabla}{i}-\mathbf{A}\right]\Delta\right]-\kappa^2\nabla\times\nabla\times\mathbf{A}\ ,$$

where $\tilde{f}(\mathbf{r},t)$ is the dimensionless random force and its correlation is given by

$$\langle\tilde{f}^*(\mathbf{r},t)\tilde{f}(\mathbf{r}',t')\rangle=\frac{1}{12}k_BT\left[\frac{H_c(0)^2}{8\pi}\xi(0)^3\right]^{-1}\times\delta(\mathbf{r}-\mathbf{r}')\delta(t-t')\ . \tag{9}$$

Let us next introduce the link variable between $\mathbf{r}_1$ and $\mathbf{r}_2$ as

$$U_\mu^{\mathbf{r}_1\mathbf{r}_2}\equiv\exp\left[\int_{\mathbf{r}_1}^{\mathbf{r}_2}A_\mu(\mathbf{r})d\mu\right]\ , \tag{10}$$

with $\mu=x,y$, where the magnetic field H is in the z direction. For computer simulations, it is convenient to discretize the system. The first derivative and the rotation of the vector potential are given by

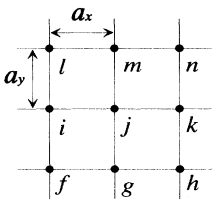

FIG. 1. Configuration of the lattice used in the simulations.

$$\left[\frac{1}{i}\frac{\partial}{\partial x}-A_x\right]\Delta\rightarrow -i\frac{U_x^{kj}\Delta_k-\Delta_j}{a_x}\ ,$$
$$B_z=(\nabla\times\mathbf{A})_z\rightarrow -\frac{i}{a_x a_y}(1-U_y^{kn}U_x^{nm}U_y^{mj}U_x^{jk})\ , \tag{11}$$

respectively, where a_x and a_y are the lattice constants in the x and y directions. Here, the superscripts and subscripts $j,k,\ldots$ denote the lattice points as shown in Fig. 1. The second derivative of Eq. (8) is discretized as

$$\left[\frac{1}{i}\frac{\partial}{\partial x}-A_x\right]^2\Delta\rightarrow\frac{U_x^{kj}\Delta_k-2\Delta_j+U_x^{ij}\Delta_i}{a_x^2}\ , \tag{12}$$

We then obtain the discretized TDGL equation from Eqs. (8)–(12) as

$$\frac{\partial\Delta_j}{\partial t}=\frac{1}{12}\left[\frac{U_x^{kj}\Delta_k-2\Delta_j+U_x^{ij}\Delta_i}{a_x^2}+\frac{U_y^{mn}\Delta_m-2\Delta_j+U_y^{gj}\Delta_g}{a_y^2}+(1-T)(|\Delta_j|^2-1)\Delta_j\right]+\tilde{f}_j(t)\ ,$$
$$\frac{\partial U_x^{jk}}{\partial t}=(1-T)\mathrm{Im}[\Delta_k^* U_x^{jk}\Delta_j]-\frac{\kappa^2}{a_y^2}\{U_x^{jk}U_y^{kn}U_x^{nm}U_y^{mj}U_x^{jk}U_y^{kh}U_x^{hg}U_y^{gj}-1\}\ , \tag{13}$$
$$\frac{\partial U_y^{jm}}{\partial t}=(1-T)\mathrm{Im}[\Delta_m^* U_y^{jm}\Delta_j]-\frac{\kappa^2}{a_x^2}\{U_y^{jm}U_x^{ml}U_y^{li}U_x^{ij}U_y^{jm}U_x^{mn}U_y^{nk}U_x^{kj}-1\}\ .$$

In Ref. 4, we have solved Eq. (8) directly without the link variable. We have checked the results of the simulations for Eq. (13) which agreed with the previous ones for Eq. (8) in the nucleation process of the superconducting state at low external magnetic fields. In this paper, the link variable is used since a better numerical convergence is obtained in high magnetic fields.

III. SIMULATION METHOD

We consider the magnetization process of type-II superconductors in an external magnetic field in the z direction and examine the time development of magnetization in the xy plane. In conventional superconductors, the fluctuation of vortices in the z direction is much smaller compared with that in the xy plane. Therefore, the two-dimensional treatment of the TDGL equation may physically be realized when the geometrical demagnetization factor[12] is neglected.

The sample we examine has the following free boundary condition for the order parameter at the surface boundary since the perpendicular component of the current density is zero at the boundary;

$$\left[\frac{\nabla}{i}-\mathbf{A}\right]\Delta\Big|_n=0\ , \tag{14}$$

where the subscript n denotes the normal direction to the surface. The value of the magnetic-flux density $\mathbf{B}$ is equal to the external magnetic field $\mathbf{H}_e=(0,0,H)$ at the surface,

$$\mathbf{B}_s\equiv(\nabla\times\mathbf{A})_s=\mathbf{H}_e\ , \tag{15}$$

where the subscript s denotes the surface. The boundary conditions (14) and (15) are rewritten in the discretized ones by using Eq. (11). The magnetic-flux density $\mathbf{B}$ and the external magnetic field $\mathbf{H}_e$ are measured in units of $H_{c2}(0)$ from Eq. (7).

The outline of the procedure of the present simulations

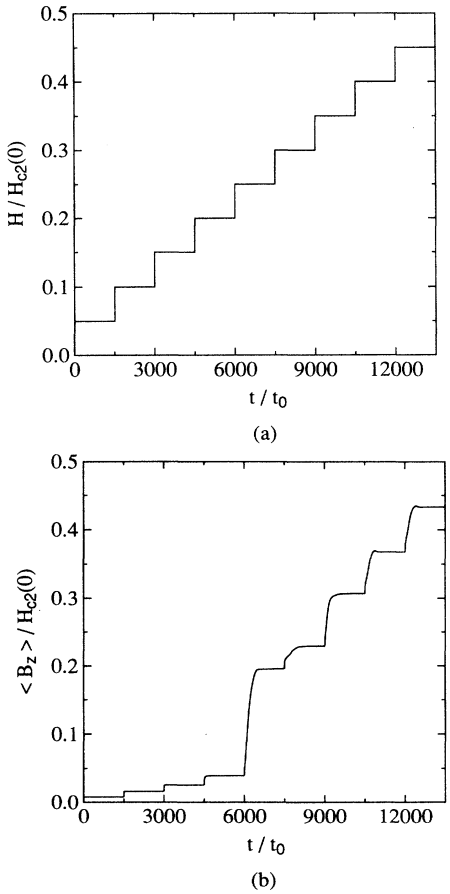

FIG. 2. (a) Time variation of the external magnetic field H in the initial magnetization process. The field is increased from $H/H_{c2}(0)=0$ to $H/H_{c2}(0)=0.45$ with the step $\Delta H/H_{c2}(0)=0.05$. (b) Time development of the magnetic induction $\langle B_z\rangle/H_{c2}(0)$, due to the external magnetic field given by Fig. 2(a).

is as follows. We use the simple Euler method for the discretized TDGL equation (13) on square lattices with N^2 lattice points, where the time step is $\Delta t=0.015$ and the lattice constants in the x and y directions are $a_x=a_y=0.5$. We set the grid size at $128\times128(N=128)$, that is, the space size is $64\xi(0)\times64\xi(0)$ in physical units. The random force $\tilde{f}_i(t)$ at each site i is independently selected from a Gaussian distribution with a zero mean. From Eq. (9) its standard deviation σ is given by

$$\sigma=\sqrt{(\Delta t/24)k_BT\{[H_c(0)^2/8\pi]\xi(0)^3\}^{-1}}$$
$$=\sqrt{(\pi E_0\Delta t/6)(T/T_c)}\ , \tag{16}$$

where E_0 is the ratio of the thermal energy to the free energy of a vortex, $E_0=k_BT_c/\varepsilon(0)\xi(0)$. Here, $\varepsilon(0)$ is the free energy of a vortex per unit length at $T=0$ and is defined by $\varepsilon(0)=4\pi\xi(0)^2[H_c(0)^2/8\pi]$. We take $\kappa=2$ and $T/T_c=0.5$. In a superconductor with $T_c=10$ K and $\xi(0)=100$ Å, for example, the sample size is ~1 μm$\times1$ μm, the characteristic time is $t_0=10^{-13}$ s, and the parameter E_0 which is a measure of the random force is $E_0=10^{-5}$. We checked the effects of the random force by changing the value of E_0. Even when E_0 is taken to be 10^{-3}, qualitatively the same results were obtained as for $E_0=10^{-5}$ except for the time scale; the time development of the order parameter becomes faster as the value of E_0 is larger. In our normalized units, the upper and lower critical magnetic fields at $T/T_c=0.5$ are given by $H_{c2}(T)=0.5$ and $H_{c1}(T)=0.04$, respectively. The initial state is taken to be a superconducting state with

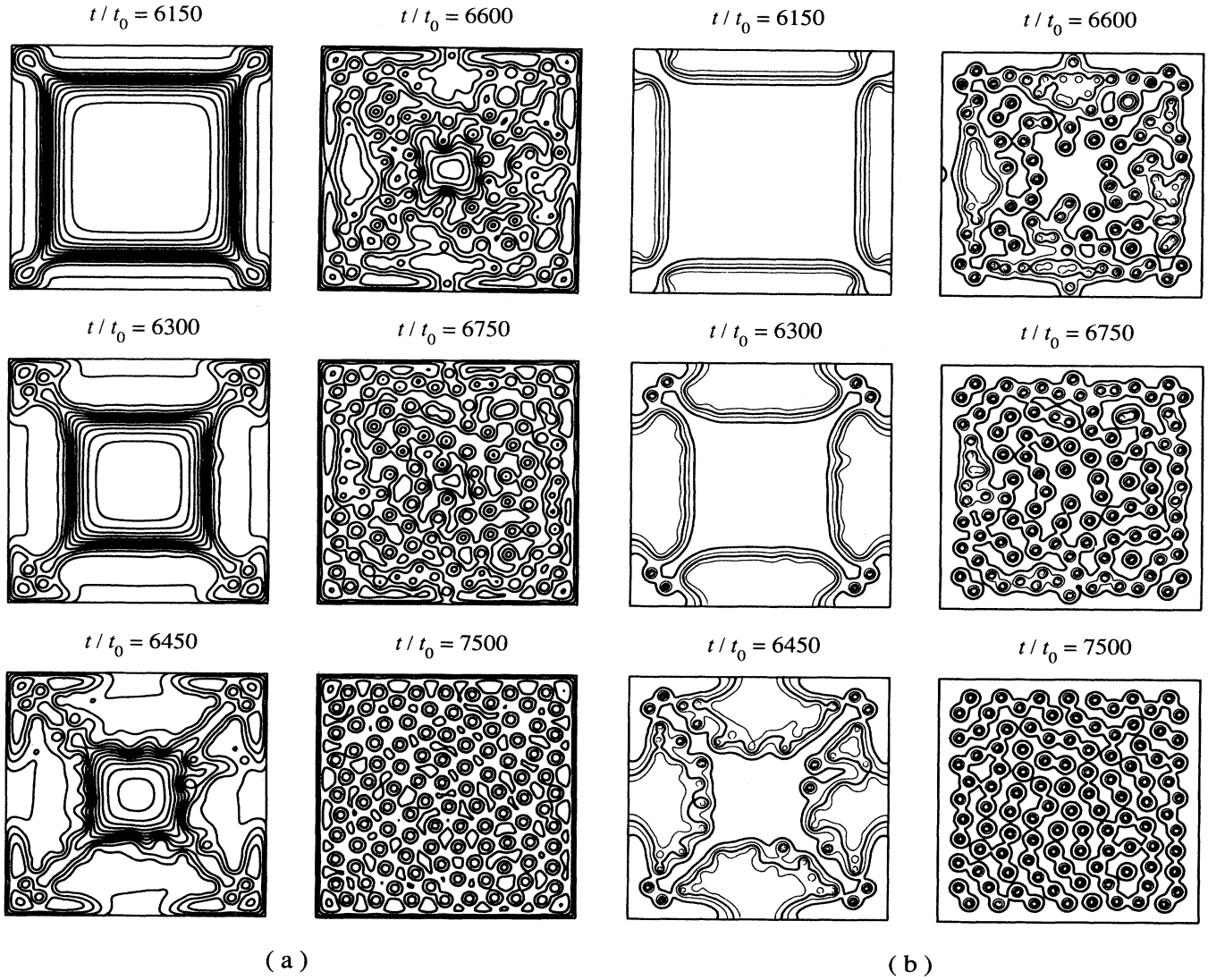

FIG. 3. (a) Time development of the magnetic-flux density $B_z(\mathbf{r})$ when the magnetic field is increased from $H/H_{c2}(0)=0.20$ to $H/H_{c2}(0)=0.25$ at $t/t_0=6000$. The contour lines with the interval 0.02 are shown. (b) Time development of the magnitude of the order-parameter $|\Delta(\mathbf{r})|$ when the magnetic field is increased from $H/H_{c2}(0)=0.20$ to $H/H_{c2}(0)=0.25$ at $t/t_0=6000$. The contour lines with the interval 0.2 are shown.

$|\Delta(\mathbf{r})|=1$ and $B_z(\mathbf{r})=0$ in the absence of the external magnetic field, i.e., a zero-field cooling (ZFC) state. Then, by numerically integrating the TDGL equation together with the Maxwell equations in various conditions, the magnetization process is simulated in Sec. IV.

IV. MAGNETIZATION PROCESS

The magnetic flux penetrates into a superconductor through the surface boundary as the external magnetic field is increased, and goes out of it through the surface boundary as the field is decreased. In order to investigate the magnetization process, we start with the initial state, with $|\Delta(\mathbf{r})|=1$ and $B_z(\mathbf{r})=0$, and increase the external magnetic field with the step $\Delta H=0.05$, as shown in Fig. 2(a). Each value of the external magnetic field is fixed for the time interval 1500. In Fig. 2(b) we show the time development of the magnetic induction $\langle B_z \rangle$, which is calculated as $\langle B_z \rangle \equiv (1/V)\int B_z(\mathbf{r})d\mathbf{r}$. The magnetic induction becomes constant in each magnetic field after the 1500 time interval. Thus this time period 1500 ($\sim 10^{-10}$ s in real units) is enough to stabilize the physical state in the system.

In Fig. 3 we show how the magnetic flux penetrates into the superconductor as the magnetic field is increased from $H=0.20$ to $H=0.25$ at the time $t=6000$. The contour lines of the magnetic-flux density with the interval

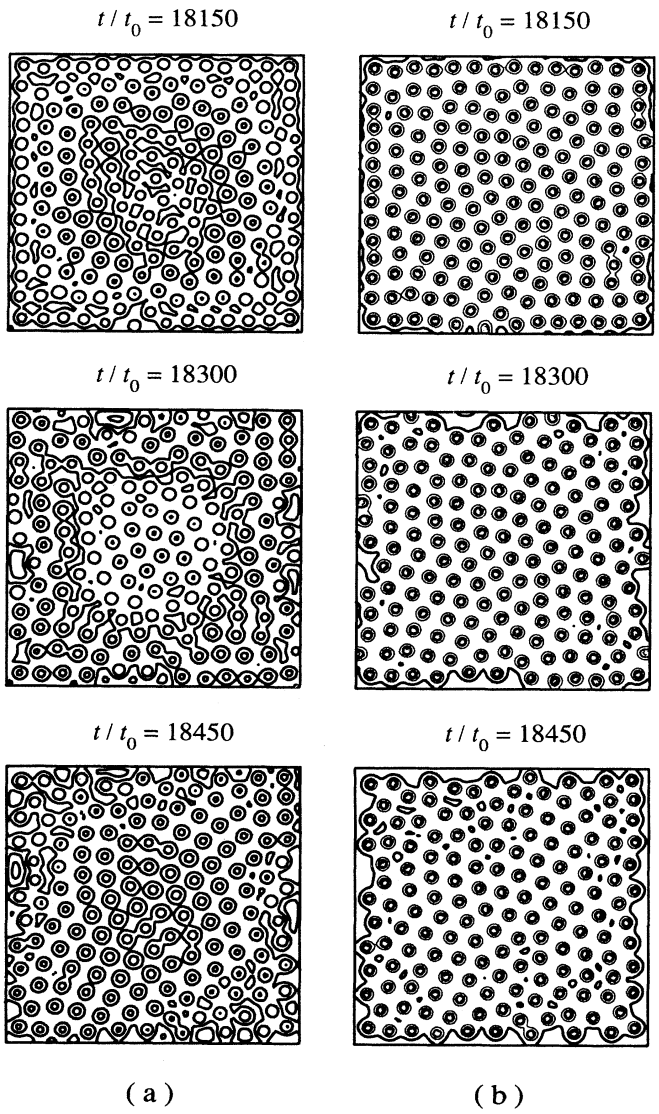

FIG. 4. (a) Time development of the magnetic-flux density $B_z(\mathbf{r})$ when the magnetic field is decreased from $H/H_{c2}(0)=0.30$ to $H/H_{c2}(0)=0.25$ at $t/t_0=18\,000$. The contour lines with the interval 0.02 are shown. (b) Time development of the magnitude of the order parameter $|\Delta(\mathbf{r})|$ when the magnetic field is decreased from $H/H_{c2}(0)=0.30$ to $H/H_{c2}(0)=0.25$ at $t/t_0=18\,000$. The contour lines with the interval 0.2 are shown.

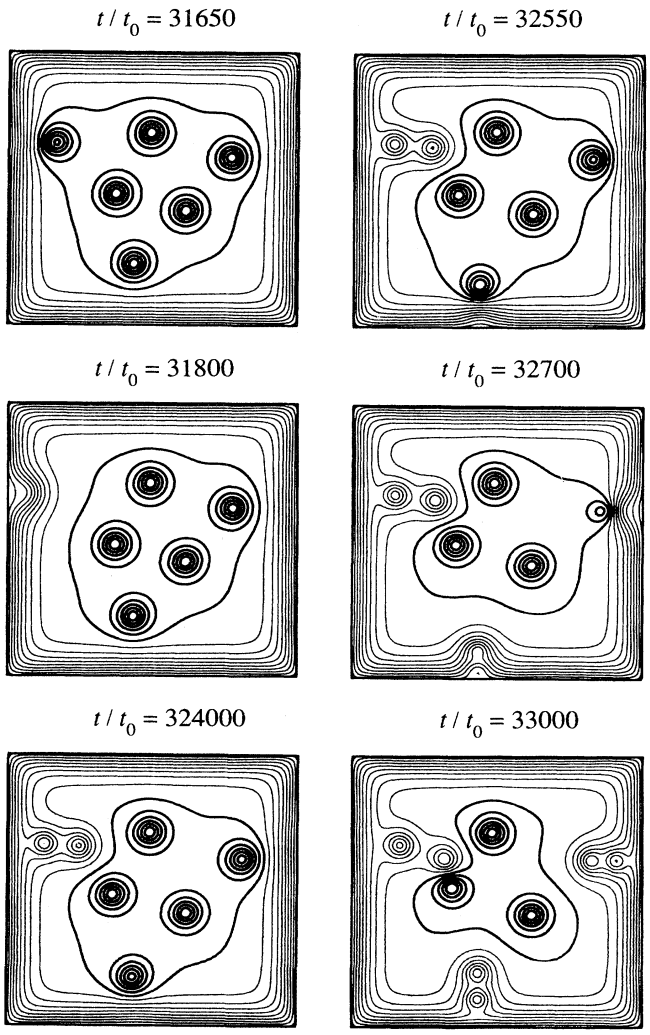

FIG. 5. Time development of the magnetic-flux density $B_z(\mathbf{r})$ when the magnetic field is decreased from $H/H_{c2}(0)=-0.15$ to $H/H_{c2}(0)=-0.20$ at $t/t_0=31\,500$. Thick and thin lines show the contours of the positive and negative magnetic-flux densities, respectively, with the interval 0.02.

0.02 and of the order parameter with the interval 0.2 are plotted in Figs. 3(a) and 3(b), respectively. At $t=6000$, the system is in the Meissner state, where the order parameter is $|\Delta(\mathbf{r})|=1$ in the system and the magnetic-flux density is $B_z(\mathbf{r})=0$ except in the range of order $\lambda(T)$ near the surface boundary. When time goes on from $t=6000$, the magnetic flux penetrates into the system from the surface boundary. However, it is not yet quantized at $t=6150$. At $t=6300$, the curvature of the magnetic flux becomes large at the edges. Then the magnetic flux is transformed into vortices. This transformation extends gradually into the system. At $t=6600$ in Fig. 3(b), several large rings are seen. At $t=6750$, these rings are divided into vortices. Thus the large rings which appear temporarily are vortices with large quantum numbers.[4] As the magnetic field was increased with the step $\Delta H=0.01$, vortices with large quantum numbers did not appear and vortices penetrated into the system one by one. This fact suggests that the magnetization process depends on the external condition.

We next examine the hysteresis curve of magnetization as the external magnetic field is reversed from $H=0.45$ to $H=-0.45$ with the step $\Delta H=-0.05$ and then increased again to $H=0.45$ with the step $\Delta H=0.05$ with each time interval 1500. Figure 4 shows how vortices go out of the superconductor at $H=0.25$, as the field is decreased from $H=0.30$ to $H=0.25$ at $t=18\,000$. In Figs. 4(a) and 4(b), the contour lines of the magnetic-flux density with the interval 0.02 and of the order parameter with the interval 0.2 are plotted, respectively. At $t=18\,000$, the mixed state is disturbed and vortices go out of the system through the surface boundary one by one. This situation is seen in the figures at $t=18\,150$ and $18\,300$. Since the magnetic-flux density is low near the surface boundary, vortices move along the density gradient.

In Fig. 5, the time development of the magnetic flux is plotted as H is decreased from $H=-0.15$ to $H=-0.20$ with the step $\Delta H=-0.05$ at $t=31\,500$, where thin and thick contour lines indicate negative and positive values of the magnetic-flux density, respectively. The interval of the contour lines is 0.02. At $t=31\,500$, there are six vortices in the system and the magnetic flux with the negative sign penetrates into the region of order $\lambda(T)$ from the surface boundary. At $t=31\,650$ a positive vortex is absorbed into the negative flux region. As soon as it disappears, antivortices (vortices with negative flux) are nucleated at the same position. We observe that vortices at the center are annihilated together with penetrating antivortices at $t=33\,000$. We also find that antivortices penetrate into the system wherever vortices go out.

V. HYSTERESIS CURVE

The hysteresis curve of magnetization is calculated as follows. The external magnetic field is increased from $H=0$ to $H=0.45$ with the step $\Delta H=0.05$, and decreased from $H=0.45$ to $H=-0.45$ with the step $\Delta H=-0.05$. Then, it is again increased to $H=0.45$ with the step $\Delta H=0.05$. In Fig. 6, the magnetic induction $\langle B_z\rangle$ and the magnetization M vs the external magnetic field are plotted, where the magnetization M is given by

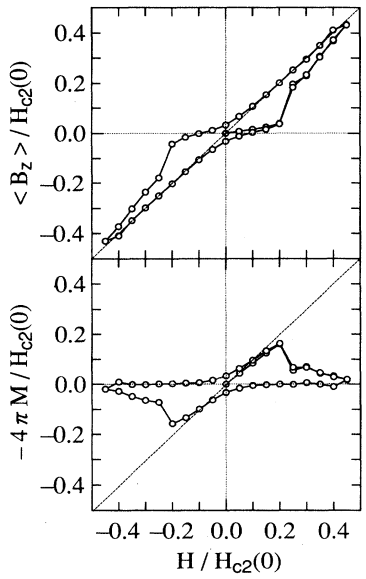

FIG. 6. Hysteresis curves of the magnetic induction $\langle B_z\rangle$ (upper part) and the magnetization M (lower part) vs the external magnetic field.

$M\equiv(1/4\pi)(\langle B_z\rangle-H)$. In the initial magnetization process, the superconductor is in the Meissner state. As the magnetic field is applied, the magnetic flux penetrates into the region of order $\lambda(T)$ near the surface boundary. As the magnetic field is further increased, the magnetization curve shows a peak at $H_p=0.20$. This field is much larger than the lower critical field $H_{c1}=0.04$. The system is in the mixed state for $H>H_p$. Once the system is magnetized, the state is complicated even for $|H|\leq H_p$; when the magnetic field is decreased from H_p and reversed, the magnetic flux in the region of order $\lambda(T)$ near the surface boundary is opposite to that of vortices in the system. As the field is further decreased to $H<-H_p$, the magnetic flux near the surface boundary is transformed into vortices. Then they penetrate into the system.

Bean and Livingston[7] have proposed the magnetic field H_s, at which vortices begin to enter into the sample through its surface boundary. In the following discussion we use physical (dimensional) units. To evaluate H_s, two forces acting on a vortex near the surface are examined, one being an image force which is attractive to the surface. The energy E_a per unit length of a vortex is given by

$$E_a(x)=\varepsilon-\left[\frac{\Phi_0}{4\pi\lambda}\right]^2 K_0\left[\frac{2x}{\lambda}\right], \tag{17}$$

where Φ_0 is the flux quantum ($=\hbar c/2e$) and K_0 is a modified Bessel function of the second kind. Here, ε is the energy per unit length of a vortex far from the surface and is approximately equal to

$$\varepsilon=\left[\frac{\Phi_0}{4\pi\lambda}\right]^2 \ln\kappa\ . \tag{18}$$

The other is the force caused by the external magnetic field H'. The field penetrates into the superconductor as $H'e^{-x/\lambda}$. If this field is of the same sign as the vortex, a repulsive force from the surface, is produced. The energy E_r is given by

$$E_r(x)=\frac{\Phi_0}{4\pi}H'e^{-x/\lambda}\ . \tag{19}$$

Thus, we obtain the total energy $E(x)$ as

$$E(x)=\left[\frac{\Phi_0}{4\pi\lambda}\right]^2\ln\kappa-\left[\frac{\Phi_0}{4\pi\lambda}\right]^2 K_0\left[\frac{2x}{\lambda}\right]+\frac{\Phi_0}{4\pi}H'e^{-x/\lambda}\ . \tag{20}$$

The energy $E(x)$ has a maximum near the surface. Let us define H_s as the magnetic field at which $E(x)$ becomes maximum at $x=\xi(T)$. Differentiating Eq. (20) with respect to x and substituting $\xi(T)$ for x, we obtain

$$\frac{H_s}{H_{c2}(0)}\equiv\frac{1}{\kappa^2}\left[1-\frac{T}{T_c}\right]e^{1/\kappa}K_1\left[\frac{2}{\kappa}\right]\sim\frac{1}{2\kappa}\left[1-\frac{T}{T_c}\right], \tag{21}$$

where K_1 is a modified Bessel function of the first kind. We evaluate H_s for $\kappa=2$ and $T/T_c=0.5$, and obtain $H_s/H_{c2}(0)=0.12$. The value of H_s is close to H_p. Thus, we identify H_p obtained in the simulations to be the surface pinning field.

We also find the second peak at $H=0.3$ in the initial magnetization curve in Fig. 6. However, the second peak disappears when the external magnetic field is increased with the step $\Delta H=0.01$. This suggests that since the redistribution of the flux is slow, the apparent hysteresis curve depends on the variation of the magnetic field.

The cross sections of the spatial pattern of the order parameter, the magnetic induction, and the y component of the current density $j_y=(\kappa^2\nabla\times\nabla\times\mathbf{A})_y$ in various external magnetic fields are shown in Figs. 7, 8 and 9, respectively.

In $H\leq 0.2$, the system is in the Meissner state. The order parameter in Fig. 7 is $|\Delta|=1$ in the system except for the surface region. The magnetic flux penetrates into the region of order $\lambda(T)$ from the surface boundary in Fig. 8, and the supercurrent rotates near the edge of the system as shown in Fig. 9.

In $H\geq 0.25$, vortices penetrate into the system as shown in Fig. 8. As the external magnetic field is increased, the spatial pattern of the magnetic-flux density tends to become uniform. The value of the order parameter is zero at the positions where the current density j_y changes sign, as shown in Fig. 9. In the system with high vortex density, vortices do not move independently but move as a bundle. In high magnetic fields, the value of the order parameter is larger near the edge than in the center (see Fig. 7). In Fig. 9 the maximum value of j is given by $j_{\max}/j_0=0.18$ at $H=0.35$ with $j_0=cH_c(0)/2\sqrt{2\pi}\lambda(0)$. This value is close to the GL critical current density[13] which is defined by

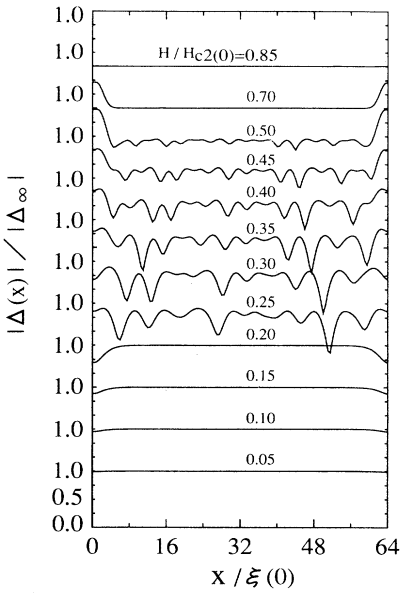

FIG. 7. The cross sections of the magnitude of the order parameter $|\Delta(x)|$ at various choices of the external magnetic field, where the surface boundaries are at $x/\xi(0)=0$ and 64. The order parameter is normalized by the equilibrium value in the absence of the magnetic field Δ_∞.

$$j_c=\frac{2cH_c(0)}{3\sqrt{3}\lambda(0)}\left[1-\frac{T}{T_c}\right]^{3/2},$$

i.e., $j_{\max}/j_c=1.3$.

Finally, we examine the surface superconducting state in $H>H_{c2}$. Saint-James and de Gennes[8] have obtained the surface critical field H_{c3} as

$$H_{c3}(T)=1.695\left[1-\frac{T}{T_c}\right]. \tag{22}$$

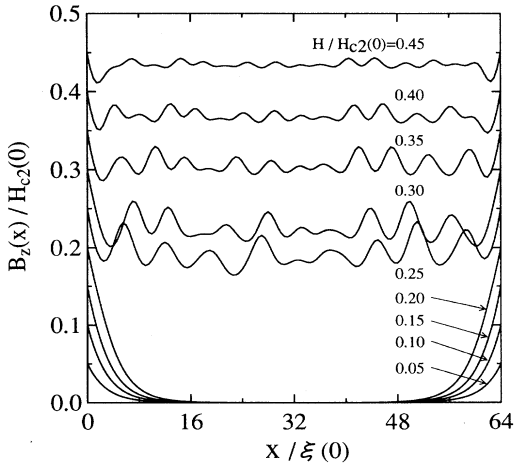

FIG. 8. The cross sections of the magnetic-flux density $B_z(x)$ at various choices of the external magnetic field, where the surface boundaries are at $x/\xi(0)=0$ and 64.

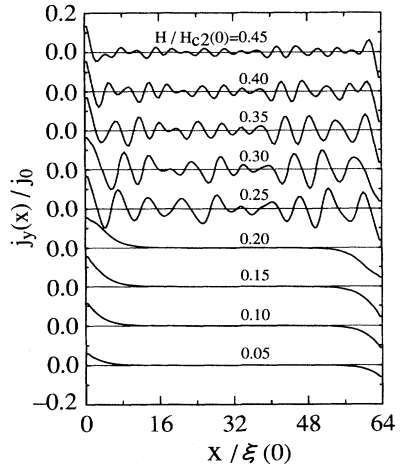

FIG. 9. The cross sections of the y component of the current density $j_y(x)$ at various choices of the external magnetic field, where the surface boundaries are at $x/\xi(0)=0$ and 64. The maximum value is obtained to be $j/j_0=0.18$ at $H/H_{c2}(0)=0.35$ with $j_0=cH_c(0)/2\sqrt{2}\pi\lambda(0)$.

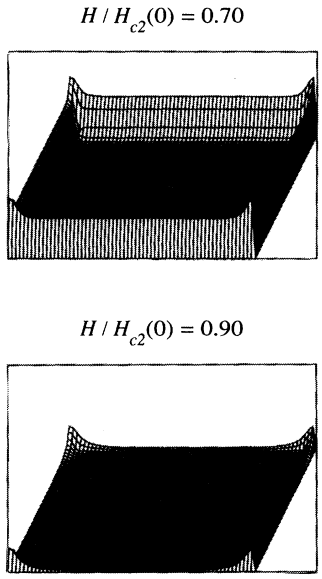

FIG. 10. The spatial patterns of the order parameter $|\Delta(\mathbf{r})|$ at $H/H_{c2}(0)=0.70$, and 0.90, where the maximum value of $|\Delta(\mathbf{r})|$ is normalized to 1.

The value of H_{c3} for our parameter values is given by $H_{c3}=0.85$. As shown in Figs. 7 and 10, there exists the superconducting surface sheath of thickness $\sim\xi(T)$ at $H=0.70$ $(>H_{c2})$. In addition, we find that even in $H=0.90$ $(>H_{c3})$ the order parameter is finite at the edges. Such edge states disappear at $H=1.00$ $(=2H_{c2})$. This it is possible that the superconducting edge states give various anomalous phenomena in high magnetic fields.

VI. SUMMARY

We have solved the TDGL equation of type-II superconductors numerically in magnetic fields. As the magnetic fields is increased from $H=0$ to $H=H_p$, the magnetic flux near the surface boundary is transformed into vortices and penetrates into the system. This field H_p, at which the mixed state appears, is the surface pinning field and much larger than the lower critical field H_{c1}. Once the system is magnetized in the field $H>H_p$, the superconducting state is complicated for $|H|\leq H_p$. We have examined the magnetization process as a function of the magnetic field and its time variation, and shown that the hysteresis curve of magnetization is sensitively dependent on the magnetization process.

We have also found that in addition to the surface superconducting state mentioned above, in the upper critical field H_{c2}, edge states exist. The edge states remain even above the surface critical field H_{c3}. Therefore it is possible that the states cause anomalous phenomena in the experiments in high magnetic fields.

We have presented computer simulations of the dynamics of the superconducting states in magnetic fields. This method can be applied to the other superconducting problems such as the dynamics of vortex lattice and flux flow in the superconductor with impurities. Such problems will be studied and presented in a separate publication.

ACKNOWLEDGMENTS

The authors are grateful to Professor S. Sawada for a number of useful comments on numerical methods. This work has been supported by Grant-in-Aid for the Ministry of Education, Science and Culture of Japan, and New Energy and Industrial Technology Development Organization under the management of the R&D of Basic Technology for Future Industries.

*Present address: Department of Physics, Nagoya Institute of Technology, Gokiso, Nagoya 466, Japan.

[1]M. M. Doria, J. E. Gubernatis, and D. Rainer, Phys. Rev. B **41**, 6335 (1990).
[2]Y. Enomoto, R. Kato, K. Katsumi, and S. Maekawa, Physica C **192**, 166 (1992).
[3]H. J. Jensen, A. Brass, A. C. Shi, and A. J. Berlinsky, Phys. Rev. B **41**, 6394 (1990).
[4]R. Kato, Y. Enomoto, and S. Maekawa, Phys. Rev. B **44**, 6916 (1991).
[5]H. Frahm, S. Ullah, and A. T. Dorsey, Phys. Rev. Lett. **66**, 3067 (1990).
[6]F. Liu, M. Mondello, and N. Goldenfeld, Phys. Rev. Lett. **66**, 3071 (1990).
[7]C. P. Bean and J. D. Livingston, Phys. Rev. Lett. **12**, 14 (1964).
[8]D. Saint-James and P. G. de Gennes, Phys. Lett. **7**, 306 (1963).

[9]C. R. Hu and R. S. Thompson, Phys. Rev. B **6**, 110 (1968).
[10]A. Schmid, Phys. Rev. **180**, 527 (1969).
[11]A. Schmid, Phys. Condens. Matter **5**, 302 (1966).
[12]See, for example, A. L. Fetter and P. C. Hohenberg, in *Superconductivity,* edited by R. D. Parks (Marcel Dekker, New York, 1969), p. 817.
[13]See, for example, M. Tinkham, in *Introduction to Superconductivity* (McGraw-Hill, New York, 1975), p. 117.